Polymer Degradation and Stability 163 (2019) 110–121

Contents lists available at ScienceDirect

Polymer Degradation and Stability

journal homepage: www.elsevier.com/locate/polydegstab

Synthesis and thermo-mechanical properties of novel spirobiindane based epoxy nanocomposites with tryptophan as a green hardener: Curing kinetics using model free approach

Pitchaimari Gnanasekar [a], Ning Yan [a, b, *]

[a] University of Toronto, Department of Chemical Engineering and Applied Chemistry, 200 College Street, Toronto, ON, M5S 3E5, Canada
[b] University of Toronto, Faculty of Forestry, 33 Willcocks Street, Toronto, ON, M5S 3B3, Canada

ARTICLE INFO

Article history:
Received 20 December 2018
Received in revised form
21 February 2019
Accepted 2 March 2019
Available online 6 March 2019

Keywords:
Epoxy resin
Aminoacid
Nanocomposites
Curing
Thermal and mechanical properties

ABSTRACT

In this study, novel spirobiindane based tetrafunctional epoxy resin (SBIE) was synthesized using 3,3,3′,3′-tetramethyl-1,1′-spirobiindane-5,5′,6,6′-tetraol reacting with epichlorohydrin. The molecular structure of the synthesized resin was characterized by Fourier transform infrared spectra (FTIR) and ^{1}H and ^{13}C Nuclear magnetic resonance spectra (NMR). The blends of SBIE with different proportions (2, 4, 6, 8 and 10 wt%) of montmorrilonite nanoclay (MMT) were prepared using ultrasonication process. The quality of dispersion and intercalation/exfoliation of the cured epoxy nanocomposites were analyzed by X-ray diffraction (XRD) and scanning electron microscope (SEM) studies. The curing reactions between SBIE and tryptophan, as an environmentally friendly curing agent, in the presence of 2,4,5-triphenylimidazole together with their nanocomposites including MMT were examined. Curing kinetic studies of the SBIE epoxy matrix and nanocomposites were characterized by differential scanning calorimetry (DSC) at different heating rates (10, 20 and 30 °C/min). Flynn-Wall-Ozava (FWO) and Vyzovkin (VYZ) methods were used to calculate the activation energies (Ea). The thermal degradation behaviour of the cured nanocomposites was investigated by using a thermogravimetric analyser (TGA). Moreover, the lap joint shear bonding strengths of SBIE/MMT nanocomposites were investigated. It was found that a significant improvement in thermomechanical performance of the resultant epoxy nanocomposites was obtained when compared to those of the neat epoxy matrices.

1. Introduction

Epoxy resins are used in a wide range of industrial applications, including adhesives, construction materials, composites, laminates, coatings, etc., owing to their high strength, low viscosity, low volatility, low shrinkage during cure, low degree of creep, and good adhesion to many substrates [1]. Among various epoxy resins, tetra functional epoxy resins have an excellent combination of chemical and corrosion resistance, and good mechanical and electrical properties [2]. But the brittle characteristics of the tetra functional resins limit their usage in many applications, such as in aerospace and automotive industries. Therefore, a significant effort has been made to improve the toughness of the epoxy systems in recent decades [3,4]. There is a strong demand for high performance tetraglycidyl epoxy resins with excellent stiffness and toughness. Therefore, structural modification of epoxy resins together with suitable nano reinforcements for achieving enhanced thermal and mechanical properties are explored [5–7].

Epoxy resins can be generally divided into three types depending on the crosslinking reactions during curing. These includes: 1) free radical polymerization; 2) condensation reaction; and 3) addition reaction. In all types of curing reactions, the epoxy resin releases heat in an exothermic reaction as it forms a three-dimensional network with a curing agent, or hardener, (which is typically a type of polyamines, polyamides, anhydrides or mercaptants) [8,9]. It is worth noting that the most commonly used hardeners for epoxy, such as aliphatic amine, cycloaliphatic amine, and anhydride curing agents, may cause irritation or damage to skin, eyes, and lungs [10]. Some aromatic amines can cause harm to organs and modify the oxygen carrying process in blood [11]. These potential health hazards is a concern even in the final cured

* Corresponding author. University of Toronto, Department of Chemical Engineering and Applied Chemistry, 200 College Street, Toronto, ON, M5S 3E5, Canada.
E-mail address: ning.yan@utoronto.ca (N. Yan).

https://doi.org/10.1016/j.polymdegradstab.2019.03.001
0141-3910/

products since excess unreacted residues might potentially be leached out of the product during usage. Thus, finding an alternative sustainable and low-toxic curing agent derived from nature materials is highly appealing.

Amino acids, possessing both carboxyl and amino groups, are being explored as novel curing agents for developing eco-friendly epoxy adhesives [12]. Over 500 amino acids have been found in nature, of which only 20 commonly occur in proteins. Meanwhile, lysine and tryptophan [13,14] are two amino acids have been studied as eco-friendly cross-linking agents for epoxy resins. Both amino acids possess amino and carboxyl functional groups and are able to ring open an epoxy moiety. However, tryptophan is found to be more reactive than lysine due to presence of an active hydrogen. Hence, we choose to investigate tryptophan as a green epoxy curing agent in this study.

Previous research has studied an environmentally friendly hardener, tryptophan, which is an essential amino acid, for electronics applications [14]. Motahari et al. [13] investigated curing kinetics of the reactions between diglycidyl ether of bisphenol-A (DGEBA) and tryptophan in the presence of 2,4,5-triphenylimidazole, and revealed the curing mechanism by the FTIR analysis and thermal properties of the cured resins. In order to have a wide application of this type of environmental-friendly cross-linker, a better understanding of the mechanisms and kinetics involved in its curing reactions is needed. Also, systematic investigation of the thermal and mechanical properties of the resulting cured epoxy system is also necessary.

Montmorillonite (MMT) clay is one of the most commonly used layered silicate clays for preparing polymer nanocomposites because of its larger active surface area (700–800 m^2/g) [15] and moderately negative surface charge (cation-exchange capacity). Nanoclays have long been used as a filler in polymer composites because of their low cost and their potential for improved thermal and mechanical properties [16]. Among the different types of nanoclays applied in epoxy nanocomposites, MMT clay is most attractive since it has a high aspect ratio, desirable plate morphology, large natural availability and low cost. More importantly, when compared to other nanocomposites of nano-sized fillers, such as TiO2, SiO2, Aluminium silicate, Sodium bentonite, carbon black, etc. [17], it was found that in epoxy MMT clay nanocomposites, MMT clays can be exfoliated into 1 nm thick platelets avoiding the aggregation problem that usually exists in dispersion of nanoclay in polymer nanocomposites. Some researchers [17,18] examined the effect of montmorillonite nanoclay addition to diglycidyl ether of bisphenol A type of epoxy resin (DGEBA) systems. They obtained inadequate thermal and mechanical properties as required by high performance structural products. Hence, structural modifications of the epoxy resins through incorporation of desirable atoms and groups into the backbone of the molecular chain using suitable modifiers, such as phosphorus, sulphone, silicone, polyhedral oligomeric silsesquioxanes and nanoclay, are required in order to achieve higher performance.

Research has shown that skeletal modified tera functional epoxy resins had excellent thermal and mechanical properties [19]. The introduction of spirobiindane structure into the backbone of the epoxy resin resulted in the addition of two adjacent rings orthogonal to one another connected with a tetrahedral bonding atom. Such a structure can reduce the main chain scission at high temperatures due to presence of multiband, thereby it is able to achieve highly thermal stable epoxy structure. And the tetrafunctional oxirane ring can provide superior mechanical properties [20]. Hence, in this research work, we plan to explore skeletally modification of the backbone of tetra functional epoxy resin with spirobiindane moiety for performance enhancement. We will also study the reinforcing potential of adding montmorrilonite nanoclay (MMT) as well as the application of tryptophan as the cross linker. To the best of our knowledge, spirobiindane tetrafunctional epoxy has not been investigated in the literature before.

For epoxy systems, cross linking reaction during the curing plays an important role in affecting its performance. Thermal analysis techniques are the most widely used method to characterize the curing process of epoxy systems [20–22]. Currently, there is no report on the kinetic study and thermo-mechanical properties of spirobiindane based epoxy resin system, particularly cured with a green hardener, such as tryptophan. Moreover, studies on the effect of nanoparticle addition on the curing mechanism of epoxy are limited. For kinetic modelling, Flynn-Wall-Ozawa (FWO) and Vyazkovin (VYZ) method [23–26] are based on model-free approach using isoconversion method. Hence in the present investigation, the apparent activation energy (Ea) for the curing reaction of the SBIE-montmorillonite nanocomposites are obtained using the model-free kinetic FWO and VYZ methods. The results obtained are used to gain a better understanding of the curing behaviour and to establish the appropriate curing schedule.

2. Experimental and analytical methods

2.1. Materials

3,3,3′,3′-Tetramethyl-1,1′-spirobiindane-5,5′,6,6′-tetraol (99%), and epichlorohydrin were supplied from Parachem. Benzyl triethylammonium chloride (99%), sodium hydroxide (97%), ethyl acetate, 2,4,5-triphenylimidazole, L-Tryptophan and aluminium pillared montmorrilonite clay were purchased from Sigma Aldrich. L-Tryptophan was ground into a fine powder. All the other chemicals were used without further treatments.

2.2. Blend nomenclature

Blends are labelled as SBIE, SBIE-M2, SBIE-M4, SBIE-M6, SBIE-M8 and SBIE-M10. where 2, 4, 8, 6 and 10 correspond to the weight (wt) % of nanoclay in the system, i.e. for example, blend SBIE-M2 has 2 wt % nanoclay and 98 wt% SBIE epoxy resin.

2.3. Fourier Transfer Infrared spectra (FTIR)

Fourier Transfer Infrared (FTIR) spectra for SBIE and the resulting nanocomposites were recorded on a Bruker Tensor 27 spectrometer (Bruker Optik GMbH, Ettlingen, Germany) by the KBr pellet method. 32 scans at a resolution of 4 cm^{-1} were set to produce a FTIR spectrum.

2.4. Nuclear magnetic resonance spectra (NMR)

^{1}H and ^{13}C nuclear magnetic resonance (NMR) spectra of neat SBIE were measured using a Agilent DD2 600 spectrometer (600 MHz, Agilent, Germany). The solvent used was dimethylsulfoxide-d6.

2.5. Differential scanning calorimeter (DSC)

Differential Scanning Calorimetry (DSC) tests were carried out using a TA DSC-Q100 (TA Instruments, USA). 2–5 mg of SBIE and their nanocomposites were sealed in high volume pans and the experiments were carried out from ambient temperature to 250 °C at different heating rates (10, 20 and 30 °C/min) under nitrogen atmosphere.

2.6. Thermogravimetric analysis (TGA)

The thermogravimetric (TG) curve for all thermally cured materials, such as SBIE, SMIE-M2, SBIE-M4, SBIE-M6, SBIE-M8 and SBIE-M10 were recorded in a TA TGA Q50 (TA Instruments, USA). The samples (nearly 6–7 mg) were placed in platinum pans and heated from ambient temperature to 800 °C at 10 °C min^{-1} in nitrogen atmosphere (balance purge = 40 mL min-1 and sample purge = 60 mL min^{-1}).

2.7. X-ray diffraction (XRD)

Wide angled X-ray diffraction (Philips X-ray Diffraction system, country) was used to study the crystallinity of the neat epoxy and nanocomposites. The samples were exposed for a period of 1.5 s for each angle of incidence (θ) using a Cu Kα X-ray source with a wavelength (λ) of 1.541E. The angle of incidence varied from 4 to 50 by steps of 0.02s. The periodical distances (d) of the main peaks were calculated according to Bragg's equation ($\lambda = 2d \sin\theta$).

2.8. Scanning electron microscopy (SEM)

Morphology of the cured epoxy nanocomposites were studied using a JEOL 6610 LV Scanning electron microscope (SEM) (JEOL 6610LV, Seal Laboratories, El Segundo, CA, USA at 15 kV. The sample surfaces were sputter coated with gold to avoid charging prior to imaging.

2.9. Lap shear bonding strength test

Lap-shear tests were carried out on a Instron universal tester (maker, model – 3667, location) according to ASTM D5868 with a crosshead speed of 13 mm/min (ASTM D5155-14, 2014). Betula alleghaniensis wood (Yellow birch) strips (101 mm in length × 25.4 mm in width × 2.5 mm in thickness) were prepared and conditioned at room temperature at ~60% relative humidity for 7 days. Then epoxy adhesives were uniformly applied on the polished bonding area with a glass rod to reach about 0.1 mm thickness. The two coated pieces of wood specimens were placed together for the adhesives to be cured at 150 °C with a pressure of 2 Mpa for 5 min. The wood specimens were gripped by two screw-type flat-plate grips and pulled at a shear rate of 13 mm/min. Wood specimens were prepared in tetraplicate and the average lap shear strength was reported.

2.10. Synthesize of spirobiindane based tetraglycidyl ether (SBIE)

Epichlorohydrin (10 mol) was added to a mixture of 3,3,3′,3′-Tetramethyl-1,1′-spirobiindane-5,5′,6,6′-tetraol (SBI) (1 mol) and triethylbenzylammonium chloride (TEBAC) (1 mol) in a three neck RB flask. The resulting solution was mixed for 1 h at room temperature and 30 min at 80 °C. After cooling to room temperature, 1600 mL of sodium hydroxide (5 mol) and triethylbenzylammonium chloride (0.2 mol) were added into the mixture and stirred for 30 min at 25 °C. Afterwards, a two-phased mixture of ethyl acetate/distilled water was added to the above mixture, followed by 5 min of further stirring. The extraction was carried out two times in an aqueous phase with ethyl acetate. Organic phase containing SBIE based epoxy resin was washed again with an aqueous solution of sodium chloride and dried over by manganese sulphate. Excess of ethyl acetate and epichlorohydrin was eliminated using a rotary evaporator (Scheme 1). The molecular formula of the resin is $C_{33}H_{38}O_8$ and the yield was found to be 95%.

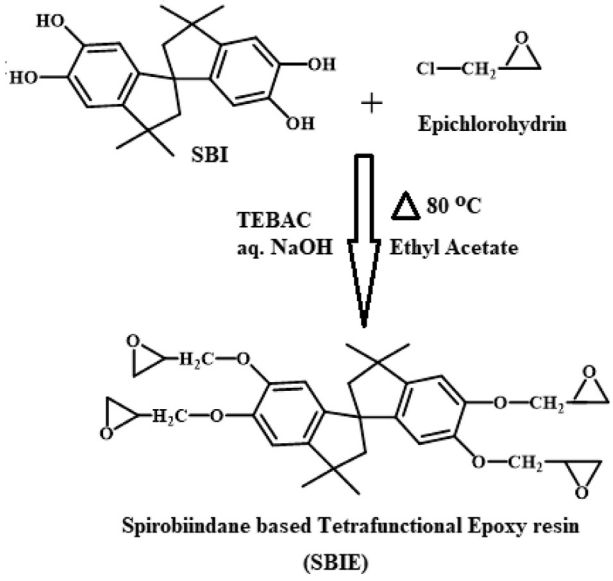

Scheme 1. Synthesize of Tetraglycidyl ether of Spirobiindane (SBIE).

2.11. Preparation of epoxy/clay nanocomposites

Spirobiindane based epoxy resin (SBIE) was dissolved in acetone. Then, the appropriate amount of tryptophan was ground well into a fine powder. With equal molar ratio it was added to the SBIE solutions followed by stirring for 30 min. 2,4,5-Triphenylimidazole catalyst at 1% relative to the total mass of SBIE/Trp was added to the mixtures while stirring. In order to prepare epoxy nanocomposite, a fixed amount of montmorrilonite clay (i.e., 2, 4, 6, 8 and 10%) was incorporated into the mixtures. After stirring for 30 min, the mixture was further mixed by ultrasonic treatment for a period of 2 h. Before curing, the acetone was evaporated under vacuum. The sample mass used for DSC analyses was around 4–6 mg.

2.12. Theory for kinetic analysis

If the curing process occurs only by the thermal method, the reaction rate (dα/dT) can be obtained by division of the peak height (dH/dT) at temperature T by the total enthalpy of the curing reaction [26], that is

$$d\alpha/dT = (dH/dT)/\Delta H_c \quad (1)$$

Where ΔHc is the total enthalpy of curing. The fractional conversion (α) can be obtained by the measurement of the partial area of the curing peak:

$$\alpha = \Delta H_T/\Delta H_c \quad (2)$$

where ΔH_T is the enthalpy of the area of the curing peak at a particular temperature.

2.12.1. Flynn-Wall-Ozawa method

The FWO method is widely used for dynamic kinetic analysis and does not require any assumptions to be made about the conversion-dependence [27]. The equation used for this method is given as follows:

$$Ea = \frac{-R}{1.052}\frac{\Delta \ln \beta}{\Delta(1/T)} \quad (3)$$

where Ea is apparent activation energy, R is the gas constant, β

is the heating rate and T is the temperature. In this method, plots of ln β versus 1/T give parallel lines for each α value. The slope of these lines give apparent activation energy, as per the expression.

$$\text{Slope} = -0.4567(\text{Ea}/\text{R}) \tag{4}$$

2.12.2. Vyazovkin method

The integration form of Arrhenius equation is given below

$$g(\alpha) = \int_0^{\alpha} \frac{d\alpha}{f(\alpha)} = A\int_0^{t} \exp\left(\frac{-Ea\ (\alpha)}{RT}\right) dt = AJ[Ea(\alpha), T] \tag{5}$$

where g(α) is the integral form of the reaction model, f(α) and T(t) is the heating program and A is the Arrhenius constant. With a linear heating rate of β = dT/dt, T(t) is linear and in eq. (5), dt can be substituted by dT/β.

$$g(\alpha) = \int_0^{\alpha} \frac{d\alpha}{f(\alpha)} = \frac{A}{\beta}\int_0^{t} \exp\left(\frac{-Ea\ (\alpha)}{RT}\right) dT = \frac{AI}{\beta}[Ea(\alpha), T] \tag{6}$$

Many authors made the numerical approximations to solve the temperature integrals (I and J) and the results of model free kinetic analysis differ widely depending on the choice of numerical approximations [28,29]. To avoid this dependence on the numerical approximation, Vyazovkin and Dollimore used the fact that for any heating rate β, g(α) is constant. Thus, with heating rates β_1, β_2 and β_3 three integrals are obtained [$g(\alpha)_{\beta 1} = g(\alpha)_{\beta 2} = g(\alpha)_{\beta 3}$].

$$\frac{A}{\beta_1} I[Ea(\alpha), T]_1 = \frac{A}{\beta_2} I[Ea(\alpha), T]_2 = \frac{A}{\beta_3} I[Ea(\alpha), T]_3$$

Consequently, A can be truncated and six equations can be formulated [30].

$$\frac{I[Ea(\alpha), T]_1 \beta_2}{I[Ea(\alpha), T]_2 \beta_1} = 1 \tag{7}$$

$$\frac{I[Ea(\alpha), T]_2 \beta_1}{I[Ea(\alpha), T]_1 \beta_2} = 1 \tag{8}$$

$$\frac{I[Ea(\alpha), T]_1 \beta_3}{I[Ea(\alpha), T]_3 \beta_1} = 1 \tag{9}$$

$$\frac{I[Ea(\alpha), T]_3 \beta_1}{I[Ea(\alpha), T]_1 \beta_3} = 1 \tag{10}$$

$$\frac{I[Ea(\alpha), T]_2 \beta_3}{I[Ea(\alpha), T]_3 \beta_2} = 1 \tag{11}$$

$$\frac{I[Ea(\alpha), T]_3 \beta_2}{I[Ea(\alpha), T]_2 \beta_3} = 1 \tag{12}$$

The summarized equation for the above is given below.

$$\sum_{i=1}^{n} \sum_{j \neq 1}^{n} \frac{I[Ea(\alpha), T]_i \beta_j}{I[Ea(\propto \alpha), T]_j \beta_i} = 6 \text{ for } n = 3 \tag{13}$$

Using the above equations, apparent activation energy for curing based on the DSC curves and for degradation based on the thermogravimetric curves for any systems can be calculated.

3. Results and discussions

3.1. FTIR and NMR studies

The FTIR spectrum of before and after polymerization of neat SBIE and its MMT clay nanocomposites (SBIE-M2, SBIE-M4, SBIE-M6, SBIE-M8 and SBIE-M10) were investigated between wavelengths of 4000–400 cm^{-1} (Fig. 1.). The characteristic absorption band present at 912 cm^{-1} suggest the presence of epoxide rings in both neat SBIE and their blended systems. The presence of epoxide rings was further supported by the appearance of peaks at 1038 cm^{-1} and 3500 cm^{-1}, which indicates C–O–C stretching of ether bond and hydroxyl group, respectively. The band noted at 1140 cm^{-1} is attributed to the –CH bending vibration of $-CH_2$ group in the spirobiindane nucleus. In addition, the peak at 2962 cm^{-1} in SBIE confirms the existence of intact spirobiindane nucleolus [31]. Therefore, it can be concluded that the FTIR spectrum of neat SBIE proves that the oxirane ring and spirobiindane nucleolus is present in the backbone chain.

In the thermally cured neat SBIE and SBIE nanocomposites, the peak pertaining to the spirobiindane nucleolus (2962 cm^{-1}) does not show any significant change. In all cured systems, the band noted at 912 cm^{-1} is nearly absent, indicating the successful opening of the oxirane ring upon the polymerization reaction. The opening of the oxirane ring was further supported by the broadened peak noted at 3500 cm^{-1}, which corresponds to the formation of hydroxyl group during the ring opening polymerization. The absorption peak noted at 834 cm^{-1} in all of the SBIE blends before and after curing was attributed to the MMT clay [14]. At low loading of nanoclay (2 wt%) there is a weak interaction noted between the nanoclay and spirobiindane nucleolus (3012 and 2962 cm^{-1}) in the cured system. As the nanoclay loading increases from 4 to 10 wt%, the peak at 296 cm^{-1} splits in to two peaks and shifts to a higher region (3012 cm^{-1}), and the intensity of band at 834 cm^{-1} is decreased [32].

The clay particles not only affect the spirobiindane nucleus, they also influence the ring opening of oxirane ring, as indicated by a new absorption band at 3124 cm^{-1} in the cured nanocomposites. This band is not shown in the neat SBIE system. Hence this observation confirms that the appearance of new band (3124 cm^{-1}) influences MMT interactions with the Oxirane ring during polymerization reaction. From the all above observations the FTIR studies concluded that the MMT clay particle affects the aromatic spacer of spirobiindane nucleus and the ring opening polymerization of oxirane ring present in the thermally cured SBIE nanocomposites.

In addition to FTIR, the structure of the synthesized neat SBIE was further investigated by ^{1}H and ^{13}C NMR and the spectra are shown in Fig. 2. In ^{1}H NMR, the appearance of peaks at 6.0–6.6 ppm (m, 16H, ArH) indicates the presence of aromatic protons in the spirobiindane structure of the neat SBIE.

The chemical shifts at 4.0–4.7 ppm correspond to the protons which are indicative of methyl groups attached in the spirobiindane skeleton. The peaks at about 2.5, 3.04–3.65 ppm show the typical oxirane absorption present in the neat SBIE. In ^{13}C NMR, the chemical shifts at 40 ppm and 50 ppm are assigned to the presence of $-OCH_2$ and –CH– of the oxirane ring present in SBIE epoxy resin, respectively [33]. The signals at 25–33 ppm correspond to the methyl group present in the spirobiindane nucleolus. The remaining shifts appearing at 119, 125, 143, 149 and 164 ppm are assigned to the aromatic carbons of spirobiindane present in the SBIE system [34]. All the above evidence indicated that confirmation of the structural elucidation of neat SBIE system having both oxirane and spirobiindane nucleus.

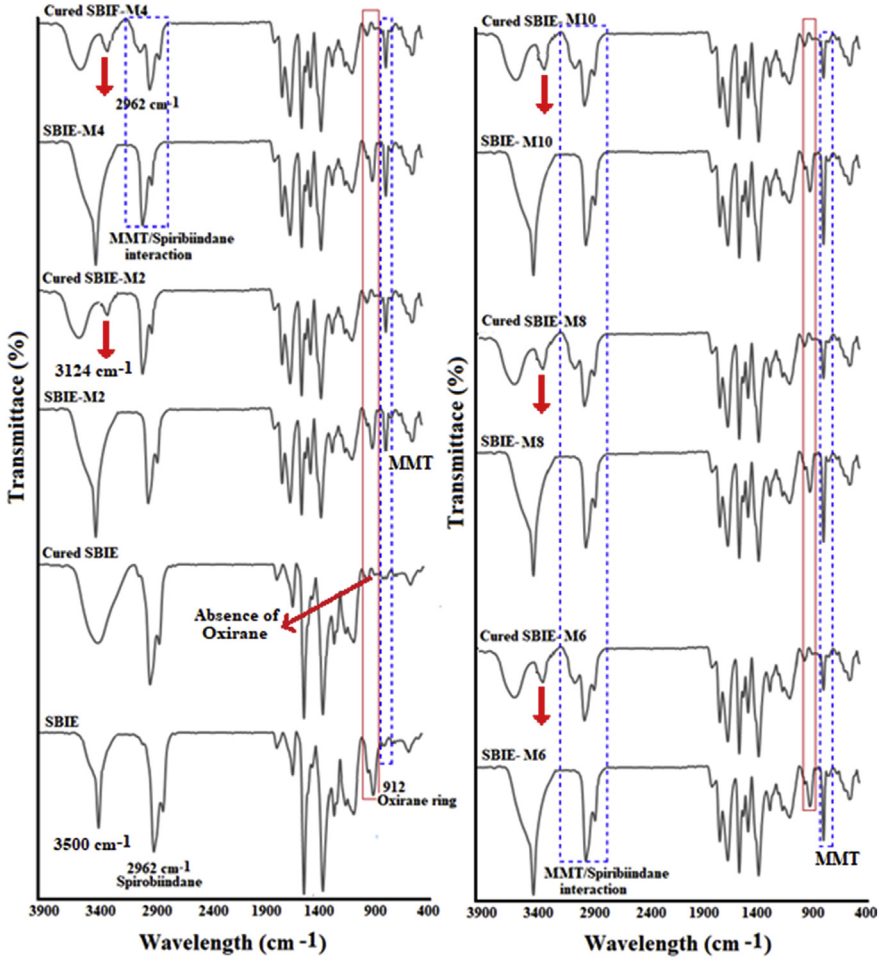

Fig. 1. FTIR Spectra of before and after cured neat SBIE and its clay nanocomposite.

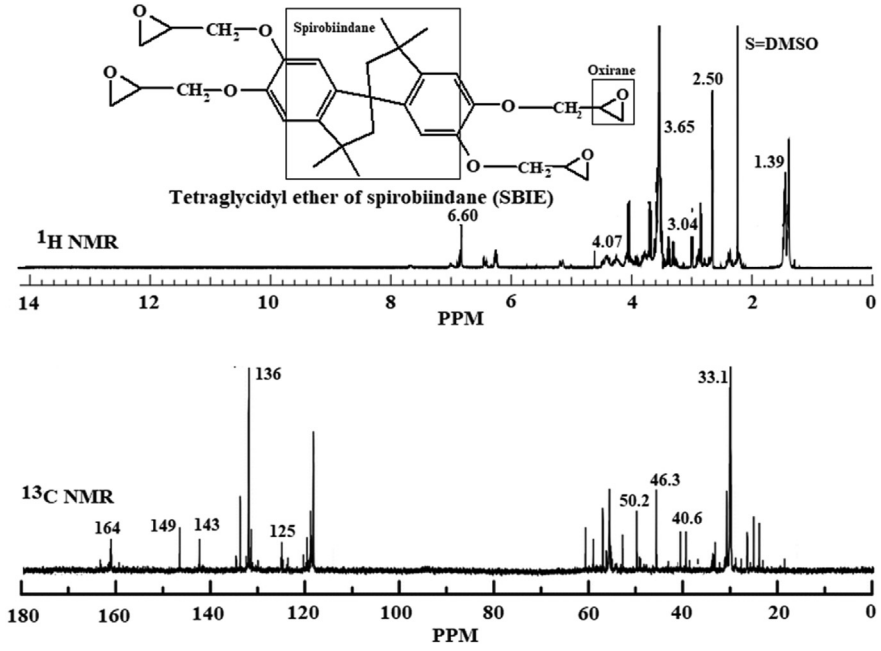

Fig. 2. ^{1}H and ^{13}C NMR Spectra of the synthesized neat SBIE.

3.2. DSC studies

3.2.1. Curing studies

The DSC curves recorded at the heating rate of (β) = 20 °C/min for SBIE and its nanocomposite are presented in Fig. 3. It is found that the SBIE and its nanocomposites underwent oxirane ring opening polymerization without phase transformation. The DSC curves and curing conversion of SBIE-M2 at different heating rates, β (10, 20, and 30 °C/min) are shown in Fig. 4,(A), and (B), respectively. For clarity, the DSC curves are shifted in the ordinate by using a common factor for each curve. The parameters such as on set temperature (T_S), end set temperature (T_E), maximum curing temperature (T_{MAX}) and enthalpy of curing (ΔH_C) derived from the DSC traces recorded at different β values for SBIE and its nanocomposites are presented in Table 1. The onset temperature (Ts) of neat SBIE curing reaction was noted at around 101 °C with the curing reaction maximum (T_{MAX}) at 152 °C and ended (T_E) at 220 °C. The enthalpy of curing (ΔH_C) and curing window were obtained as 112 J/g and 106 °C, respectively, at the heating rate of 10 °C/min. Similarly, for all the nanocomposites, SBIE-M2, SBIE-M4, SBIE-M6, SBIE-M8 and SBIE-M10, increasing the heating rate shifts the curing onset temperature to higher temperatures.

From Table 1 it is concluded that the onset of curing temperature and the intensity of exothermic peaks (Fig. 2) gradually decreases with increasing amounts of MMT clay at different heating rates. This may be due to the decrease of the concentration of epoxy resin on clay addition. The results of decreased onset temperature and curing exotherm peak for SBIE/MMT clay nanocomposites indicate that the presence of organo ions in MMT clay increases the rate of ring opening polymerization of the oxirane ring by catalytic effect [14,32]. Further clarifications of the decreased onset curing favour the amount of nanoclay fillers interacting with epoxy oligomers to result in the formation of anisotropic solution, increasing the viscosity as well as mobility of reactive species during the curing reaction [35].

The curing windows (T_E-T_S) varied with the amount of nanoclay present in the SBIE system and the profile of the curing curves of the SBIE/montmorillonite composites was similar to the shape of the curing curve recorded for neat SBIE (Fig. 3). This can be explained by the homogeneous mixing of the nanoclay into the SBIE system (ref). Further variation was noted in the enthalpy of curing (10 °C/min) of the neat SBIE (112 J/g) gradually decreasing with the amount of clay loading up to 6 wt% (SBIE-M6 ΔHc = 92 J/g).

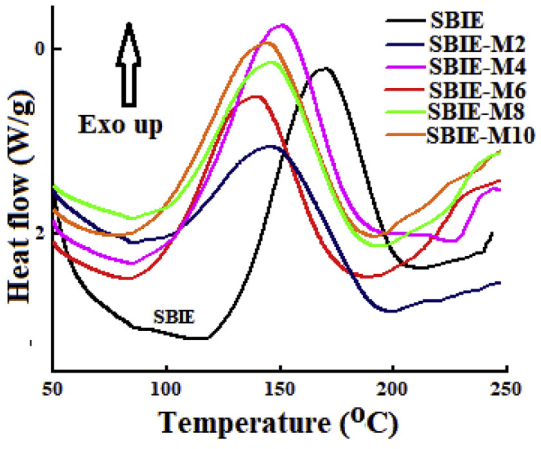

Fig. 3. DSC traces of pure SBIE and its MMT clay nanocomposites at a heating rate of 20 °C/min.

However, the enthalpy was found to increase for 8 and 10 wt% clay loadings in the SBIE system (Table 1). This observation clearly indicates that the interaction between the SBIE and MMT nanoclay particles. The primary reason for the above observations may be attributed to the confirmation stability of spirobiindane structure of SBIE and its oxirane ring was hindered by the addition of different level of nanoparticles [36]. The FTIR studies indicated the existence of interactions between the oxirane ring and spirobiindane nucleus present in the SBIE and the MMT nanoclay. Hence, it was reasonable to expect variations in the curing parameters of the SBIE-MMT nanocomposites. As to the expectations, the parameters obtained from the DSC studies discovered the influence shown by the presence of nanoclay particles in the SBIE system matrix.

3.2.2. Curing kinetics

Two different kinetic methods (FWO and VYZ) were used for the kinetic study of the curing of SBIE and its composites. The plots between apparent activation energy (Ea) and the reaction extent (α) for all samples analyzed by the FWO method are shown in Fig. 5, and the corresponding values are tabulated in Table 2. The activation energy (Ea) for SBIE was observed to increase gradually with increasing extent of reaction (α). Generally, in the curing process molecules undergo gelation (from liquid to rubber) and vitrification (from rubber to glass) transitions. According to the Table 2, the Ea values of SBIE calculated from VYZ method described that initial apparent activation energy (Ea) values for the SBIE curing increased from 49 to 69 kJ/mol as the extent of the reaction (α) value increased from 0.1 to 0.5. This may be owing to the decrease of the mobility of the reactive groups of the partially cured epoxy and the autocatalytic nature of epoxy curing [37]. Then the Ea values progressively decreased (69 kJ−50 kJ/mol) as the reaction extent level (α) reaches from 0.5 to 0.7. After that the Ea values gradually increased till the end of the curing reaction, which was related to the progress of the reaction by epoxy ring opening in different stages of the cure.

As it was studied by Mohatari et al. [37], various reaction path ways were possible during the reaction between epoxy and tryptophan in the presence of 1-cyanoethyl-2-ethyl-4-methylimidazole as a catalyst. Similarly in this study the authors explained the curing reaction between the tryptophan with 2,4,5-triphenylimidazole as a catalyst and the SBIE epoxy ring to produce zwitterion that quickly reacted with tryptophan to produce a carboxylate anion (Scheme 2). This carboxylate anion reacted with the oxirane ring producing a new alkoxide anion that causes curing reaction to progress through an anionic polymerization in the propagation step [13].

The incorporation of the MMT nanoclay in SBIE must have had some influence on the polymerization of SBIE. In Fig. 5, the trend in the apparent activation energy curves for the SBIE-M2 and BSIE-M4 are nearly same with neat SBIE. From the FTIR studies it can be concluded that the low-level loading (2 and 4 wt%) of clay content does not influence the SBIE system much, but the values for apparent activation energy are lower compared to neat SBIE system. When compared to the neat SBIE system, the presence of 6, 8 and 10 wt% of MMT in SBIE nanocomposites showed completely different behaviour and the Ea values of SBIEM-6, SBIE-M8 and SBIE-M10 seems to increase initial reaction extend level and then decreases as the polymerization proceeds. This is may be because in the initial stages of curing, the mobility of the epoxy groups in SBIE/MMT nanocomposites is higher than in the neat SBIE resin system. At later stages, the movement of segments are more restricted due to curing process and that increases the activation energy for curing.

Further, it is justified that at higher loadings of MMT (8 and 10%), the nanoparticles tend to aggregate in the neat SBIE system.

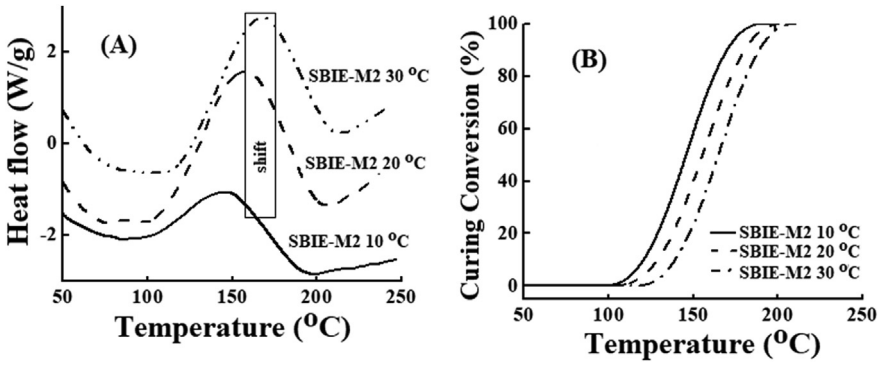

Fig. 4. A. DSC curves of SBIE-M2 at different heating rates, B: Curing conversion of SBIE-M2 at different heating rates.

Table 1
DSC Studies of SBIE and its nanocomposites at Different β Values.

Sample	Heating rate (β) °C/min	T_S (°C)	T_E (°C)	T_{MAX} (°C)	T_E-T_S (°C)	ΔH_C (Jg^{-1})
SBIE	10	101	220	152	119	112
	20	107	228	166	121	128
	30	115	237	175	122	141
SBIE-M2	10	85	197	138	112	99
	20	92	208	154	116	111
	30	98	216	163	118	120
SBIE-M4	10	82	198	148	116	94
	20	88	206	157	118	116
	30	94	211	166	117	122
SBIE-M6	10	81	194	150	113	92
	20	88	204	165	116	128
	30	96	210	177	114	143
SBIE-M8	10	82	191	144	109	98
	20	87	202	153	115	115
	30	94	209	163	115	124
SBIE-M10	10	81	190	146	109	104
	20	88	202	156	114	115
	30	93	210	165	117	123

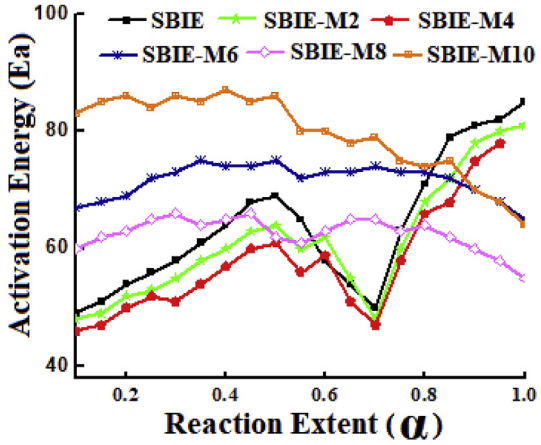

Fig. 5. DSC studies: Relative reaction extent versus apparent activation energies during curing of neat SBIE and nanocomposites systems.

Because of the presence of more clay particles, the possibility of surface interaction of spirobiindane nucleus present in SBIE with the surface of the nanoclay platelet clusters is sufficiently high at initial stages of polymerization [36]. As the polymerization proceeds, the slippage of clay platelets decreased the viscosity of the medium.

Even though the movement of the segments are restricted, the higher aggregation of clay platelets is probably favoured over the polymerization of SBIE molecules and hence, the apparent activation energy decreases in the final stage of polymerization.

3.3. XRD and SEM analysis

XRD diffraction (XRD) analysis was carried out for the neat SBIE, MMT and epoxy reinforced with different weight percentages of nanoclay and the results are presented in Fig. 6. There is variation in the peak intensity of MMT filled SBIE epoxy nanocomposites from $2\theta = 22.4°$ (MMT) to $2\theta = 19.1°$. The intensity of the peaks in this region significantly increased with increased amounts of the clay. The shift of the peaks towards a lower angle indicated that the interplanar spacing among the clay platelets was decreased and there is a presence of a mixed intercalated and exfoliated clay particles in the epoxy nanocomposites [38,39], The decrease in interplanar spacing was higher with increasing clay contents in the system, suggesting that the systems with a lower level of clay loading have more exfoliated morphology.

Similar results were observed when incorporating organically modified montmorillonite nanoclay into a polyester resin-based powder coating in the literature [40]. The expansion of the interplanar spacing caused by the high degree of intercalation of the epoxy resin within the montmorillonite galleries indicated a higher

Table 2
Apparent activation energy (Ea) at different conversion rates.

Reaction Extent (α)	Apparent Activation Energy (Ea) (kJ/mol)											
	SBIE		SBIE-M2		SBIE-M4		SBIE-M6		SBIE-M8		SBIE-M10	
	FWO	VYZ	FWO	VYZ	FWO	VYZ	FWO	VYZ	FWO	VYZ	FWO	VYZ
0.1	52	49	51	48	48	46	71	67	64	60	86	83
0.2	56	54	55	52	53	50	73	69	67	63	89	86
0.3	61	58	59	55	54	51	77	73	71	66	90	86
0.4	68	64	63	60	61	57	78	74	69	65	92	87
0.5	72	69	68	64	65	61	79	75	65	62	90	86
0.6	63	58	67	62	64	59	78	73	66	63	84	80
0.7	55	50	51	48	53	47	77	74	67	65	82	79
0.8	74	71	72	68	69	66	76	73	68	64	77	74
0.9	84	81	81	78	78	75	75	70	64	60	75	70
1.0	89	85	83	81	82	78	69	65	57	55	68	64

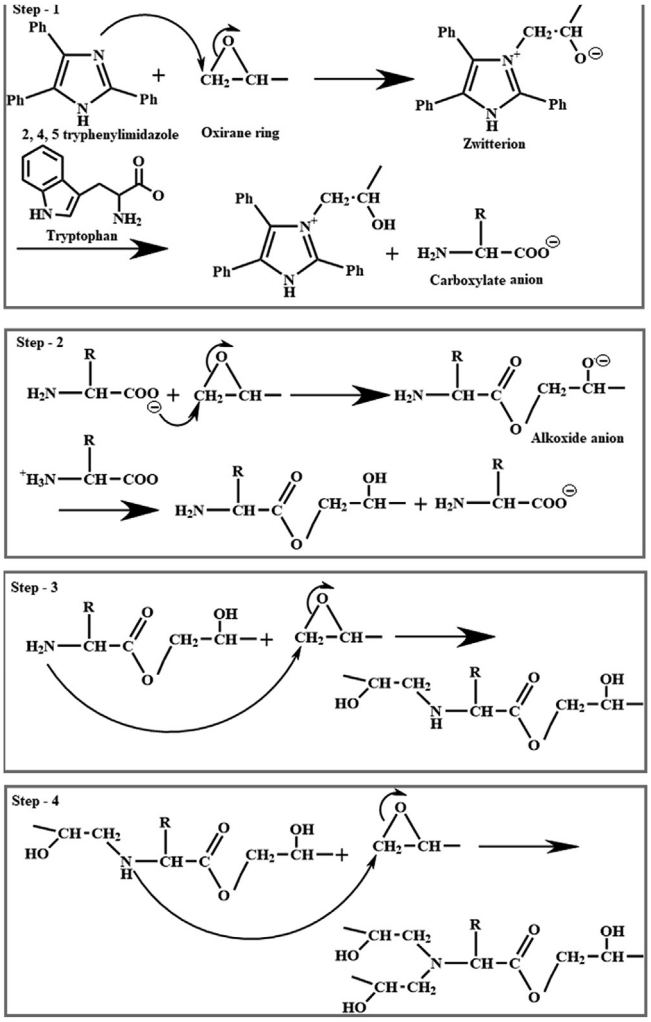

Scheme 2. The Possible mechanism for curing reaction of tetraglycidyl ether of spirobiindane (SBIE) with tryptophan in the presence of 2,4,5- triphenyl imidazole.

dispersion of the clay in the polymer matrix, thus providing evidence of predominantly exfoliated phase. Similarly, in this study, the introduction of clay particles at lower concentrations led to better clay particle dispersion within the SBIE system. However, higher levels of nanoclay loading in epoxy resin had a strong evidence of being highly exfoliated and involved interactions of nanoclay with spirobiindane nucleus and the oxirane ring leading to a decrease in the interplanar spacing between the clay platelets.

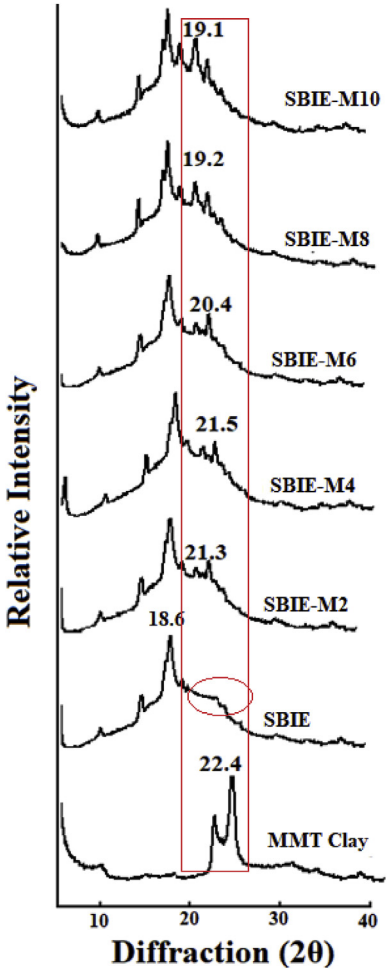

Fig. 6. XRD spectra of neat SBIE and its nanocomposites with montmorillonite nanoclay.

3.4. Morphology of the epoxy nanocomposites

The surface morphology of the cured neat SBIE and nanocomposites were studied using SEM. SEM images are shown in Fig. 7. The SEM image of the neat SBIE sample showed smooth surface free of voids. With the addition of clay particles, the surface morphology of the epoxy nanocomposites became rough. This rough surface could promote better interfacial bonding between the nanoclay fillers and epoxy resin [41]. In Fig. 7, the SEM image of

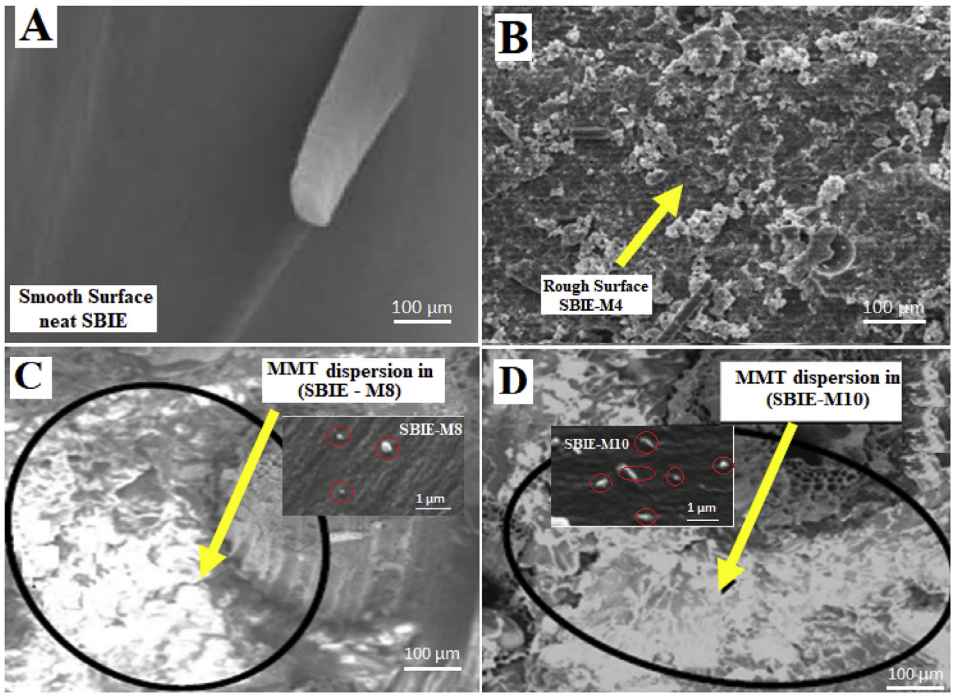

Fig. 7. SEM image of cured (A) Neat SBIE epoxy resin, (B) SBIE-M4, (C) SBIE-M8 and (D) SBIE-M10.

nanocomposite with 4 wt% of clay showed the nanoparticles were dispersed uniformly without agglomeration. It is revealed that the addition of nanoclay fillers in SBIE nanocomposites resulted in an improvement in toughness. The SBIE with a higher loading of MMT nanoparticles (8 and 10 wt%) had nanoclay on the surface and the distance between clusters were significantly large which was a good evidence for great dispersion and exfoliation. Hence, this observation proved that well dispersed nanoclay particles present in all nanocomposites allowing for the applied load to be evenly distributed to resist crack propagation in the adhesive [42].

3.5. Bonding strength

The average lap shear bonding strengths for the neat SBIE and its clay nanocomposites are shown in Fig. 8. The average dry lap shear strength increased from 2.02 MPa for neat SBIE, to 2.34, 2.41, 2.56, 3.13 and 3.62 MPa for SBIE-M2, SBIE-M4, SBIE-M6, SBIE-M8 and SBIE-M10 respectively. The results indicated that the introduction of MMT nanoclay to the neat SBIE adhesives noticeably enhanced the lap shear bonding strength. It had been shown in a previous study, the viscosity of the epoxy resin increased with the increasing percentages of nanoclay. Since both smaller contact angles and increasing viscosity are associated with less penetration in the Washburn equation [43], it can be concluded that the epoxy with 10% nanoclay did not penetrate as much in the same amount of time as the epoxy with no nanoclay. Adhesive that fully penetrated the yellow birch substrate is, by necessity, not available at the glueline, therefore the specimens with 10% nanoclay had more adhesive at the glueline than the samples without nanoclay. This difference in the amount of adhesive retained at the glueline may have contributed to the greater shear strength of the joints with 10% nanoclay. Where there is a defect of unevenness at the surface of the substrate, the adhesive with 10% nanoclay can fill in the valleys to provide a better contact at the glueline. For the adhesive without nanoclay, these valleys remain unfilled to result in a loss of joint strength [44].

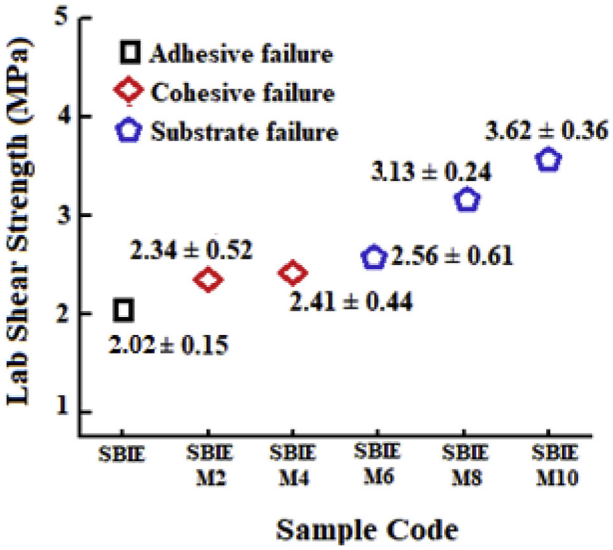

Fig. 8. The Average lap shear strength for neat SBIE and its Nanocomposites.

The SEM study reveals that the dispersion and exfoliation were seen in all nanocomposites and suggests that a clamping force will be acted onto the surface of nanoclay and so the interfacial bonding is enhanced [41]. Previous research also demonstrated that the clay concentration in nanoclay/epoxy composites played an important role in the enhancement of performance [42]. The optimal weight percentage varies in different studies. Ho et al. [45] demonstrated that the hardness of nanoclay/epoxy composite increased as clay concentration increased until an optimal weight percentage of 5%. Xi et al. [46] analyzed the electrical conductivity and the shear strength of electroconductive adhesives, prepared from polyurethane resins filled with different kinds of modified graphite's. They found that the strength of the adhesive joints on aluminium

increased up to a filler content of 20 wt%. Hence the most suitable nanoclay concentration depends on the design requirement of the application, so there is a need to find out the optimal percentage for each situation. Based on the above discussion, the authors conclude from this investigation that the newly synthesized tetrafunctional glycidyl ether of spirobiindane based epoxy wood adhesive nanocomposites seems adhesive strength increases up to at least 10% nanoclay.

This adhesion increments of the nanocomposite is supported by previous research that established nanoclay reacted with epoxy oxirane ring to form chemical bonds [47]. Because of the presence of a large number of functionality groups (epoxy/hydroxyl/ester/amine) in SBIE and nanoclay, the possible interactions may take place through hydrogen bonding, polar-polar and polar induced polar interaction. This chemical bond formation could lead to increase in the adhesive properties. The observation of this chemical bonding is correlated with the FTIR studies. Results of the failure mode analysis of the lap shear specimen after testing also further supported this argument, by showing that the adhesive containing up to 4 wt% of nanoclay exhibited adhesion failure mode instead of wood failure. Such a failure mode [48] is usually due to poor wetting by the adhesives on the substrates that is probably caused by fast skin formation.

Finally, this study concluded that this increase in strength and decrease in delamination is due to the increased amount of SBIE/MMT clay nanocomposite adhesive in the glueline. The neat SBIE adhesive with no nanoclay penetrated substrate more quickly and further than the adhesive with the nanoclay. There is more adhesive available to fill in defects at the surface of the substrate when nanoclay is added, creating a stronger bond that has a higher resistance to water penetration.

3.6. TGA studies

The TG and DTG curves for the thermally cured neat SBIE and its nanocomposites are shown in Fig. 9. The onset (T_S), maximum (T_{MAX}), endset (T_E) temperatures for the degradation and the amount of char residue obtained at 600 °C for all samples are tabulated in Table 3. Since we have already seen that nanoclay addition affected curing behaviour, it is reasonable to expect the added clay particles would also have an influence during the degradation of the cured epoxy nanocomposites. The thermally cured pure SBIE shows the onset degradation temperature at 238 °C, attaining maximum at 335 °C and then ending at 440 °C. The DTG curve of thermally cured neat SBIE shows multistage degradations overlapping each other indicating that the second degradation of the SBIE starts before the termination of the first degradation. Perhaps the incorporation of nanoclay particles in different weight levels does not affect the overlapping of the degradation stages of the cured SBIE (Fig. 9).

Table 3
Kinetic parameters during thermal degradation for the cured SBIE epoxy resin and its nanocomposites.

Sample Code	T_S (°C)	$T_{10\%}$ (°C)	T_{MAX}	T_E (°C)	Char residues (%) @ 600 (°C)
SBIE	238	246	335	440	5.1
SBIE-M2	234	251	352	480	19.3
SBIE-M4	231	258	365	482	20.3
SBIE-M6	230	261	371	488	20.8
SBIE-M8	227	266	384	495	24.1
SBIE-M10	223	271	398	497	25.9

However, the onset and endset degradation values of neat SBIE are much affected by the different levels of clay loading in the systems. From Table 2 it is revealed that cured SBIE-M2, SBIE-M4, SBIE-M6, SBIE-M8 and SBIE-M10 show that the onset and endset thermal degradation are 234–480, 231–482, 230–488, 227–495, and 223–497 °C respectively. The nanocomposites showed slightly reduced thermal stability, as indicated by a slight decrease in the onset of degradation, whilst the final endset (from 440 to 497 °C) and char concentration (5.1–25.9%) increased for greater organoclay concentrations. It is important to note that TGA curves of resin systems with and without organoclay generally show the same behaviour in the lower temperature region before the onset of degradation. A separate degradation of the interlayer exchanged ions is not observed. It is assumed that the interlayer exchanged ions are well embedded or incorporated into the polymer matrix. This is in good agreement with the degradation behaviour observed for other exfoliated epoxy organoclay nanocomposites by previous research [49]. The lower initial degradation temperatures for the nanocomposites may be related to the participation of tryptophan in the epoxy curing reaction that might be hindered by aluminium pillared montmorillonite clay and, therefore, decreased the degree of cross-linking of the epoxy. As a result, there might be some uncured tryptophan present in the system [50]. The first decomposition stage for free tryptophan occurred between 223 and 235 °C. Therefore, here initial degradation can be related to the degradation of tryptophan. Even though the nanocomposites indicate reduced thermal stability in the initial stages, the final degradation of endset and char residues are increased with increasing nanoclay content (Table 3). Hence this TGA study confirms a higher thermal stability has been achieved when increasing the clay content to the neat SBIE system.

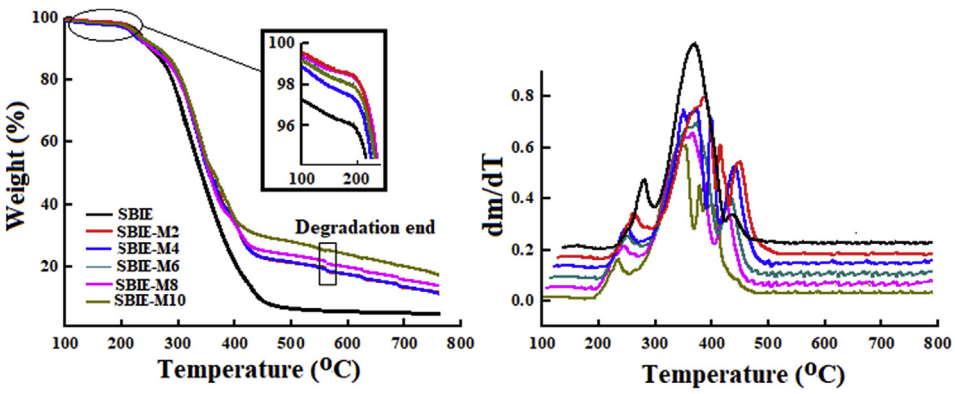

Fig. 9. TG and DTG curves of cured SBIE and its nanocomposites.

3.7. Conclusion

Novel skeletally modified spirobiindane based tetra functional epoxy resin was successfully synthesized. The developed materials were characterized by spectral studies to ascertain their structures. The study of the cure kinetics of the synthesized epoxy resin cured by tryptophan, an environmentally curing agent, showed that the incorporation of MMT nanoclay reduced the heat release and shortened the cure time. This indicated that the nanoparticles played a catalytic role in the reaction. The curing kinetics of the synthesized materials were studied using the FWO and VYZ kinetic methods, and the results obtained were similar for the two methods. For SBIE nanocomposites, Ea values increased with the increase of clay contents in the initial stage but decreased in the later stage of the curing process. It indicated that initially the viscosity of the adhesive medium was high due to the presence of nanoclay in the epoxy resin and hence it had high energy requirements for the curing process. As the reaction proceeded at higher temperatures, the viscosity of the polymerization medium decreased and the molecular chain mobility increased, which resulted in a lower Ea for the later stages of the curing. The surface morphology of the SBIE epoxy nanocomposites was investigated by XRD and SEM. It was interesting to observe that the XRD patterns of all the clay loaded SBIE nanocomposites exhibited mixed intercalated and exfoliated behaviour. SEM results showed that nanoclay was uniformly dispersed in the epoxy due to the existence of epoxide groups on the surface of nanoclay. It was also observed that upon comparing the lap shear strength properties of neat SBIE and their nanocomposites, a beneficial increase in mechanical properties for the reinforced nanocomposite systems was observed. The nanoclay reinforcement produced a significant improvement on the thermal stability and char yield of the spirobiindane tetra functional epoxy system. From the data obtained from different studies it concluded that the novel material developed in the present work could be applicable for a wide range of high performance industrial applications that require improved strength and thermal stability.

Acknowledgements

The authors like to acknowledge financial support from Ontario Centre of Excellence (OCE), Agriculture and Agri Food Canada (AAFC) VIA-Agri Project #25294, and Natural Science and Engineering Research Council of Canada (NSERC) CRD project 498926. FPinnovations is also acknowledged as the industry partner of the project..

References

[1] J. Panta, G.D. Janaki Ram, P.D. Abhijit, B. Srinivasa Rao, Effect of carbon nanofiller addition on the degradation of epoxy adhesive joints subjected to hydrothermal aging, Polym. Degrad. Stabil. 140 (2017) 84–94.
[2] Yi Cai, R. Paul, V. Nader, G. Ebru, A. Akram, Curing kinetics and mechanical properties of epoxy based coatings: the influence of added solvent, Prog. Org. Coating 124 (2018) 165–174.
[3] D.T. Jonathon, K. Masatoshi, A. Yoshihiko, Influence of network structure on the degradation of poly(ether)amine-cured epoxy resins by inorganic acid, Polym. Degrad. Stabil. 157 (2018) 153–159.
[4] A. Ruchi, M. Smita, K.N. Sanjay, High performance epoxy nanocomposite adhesive: effect of nanofillers on adhesive strength, curing and degradation kinetics, Int. J. Adhesion Adhes. 84 (2018) 238–249.
[5] H. Jianhua, S. Jiye, W. Dehua, L. Xinxing, T. Zhen, Flame retardant, mechanical properties and curing kinetics of DOPO-based epoxy resins, Polym. Degrad. Stabil. 109 (2014) 218–225.
[6] W.,P. Liu, S.V. Hoa, M. Pugh, Organoclay-modified high performance epoxy nanocomposites, Compos. Sci. Technol. 65 (2005) 307–316.
[7] B.B. Johnsen, A.J. Kinloch, R.D. Mohammed, A.C. Taylor, S. Sprenger, Toughening mechanisms of nanoparticle-modified epoxy polymers, Polymer 48 (2007) 530–541.
[8] H. Shigeo, H. Tatsuko, H. Hyoe, Curing and glass transition of epoxy resins from ester-carboxylic acid derivatives of monoand disaccharides, and alcoholysis lignin, Macromol. Symp. 224 (2005) 343–353.
[9] B. Francis, V. Lakshmana Rao, R. Ramaswamy, S. Jose, S. Thomas, K.V.S.N. Raju, Morphology, viscoelastic properties, and mechanical behavior of epoxy resin modified with hydroxyl-terminated poly (ether ether ketone) oligomer with pendent tert-butyl group, Polym. Eng. Sci. 45 (2005) 1646–1656.
[10] T.L. Fishback, C.R. McMillin, M.F. Farona, A new non-toxic, curing agent for synthetic polyolefins, Bio Med. Mater. Eng. 2 (1992) 83–87.
[11] P. Bastian, Occupational hepatitis caused by methylenedianiline, Med. J. Aust. 141 (1984) 533–535.
[12] Y. Li, F. Xiao, K. Moon, C.P. Wong, Novel curing agent for lead-free electronics: amino acid, J. Polym. Sci., Part A: Polym. Chem. 44 (2006) 1020–1027.
[13] A. Motahari, A. Omrania, A.A. Rostamia, M. Ehsani, Preparation and characterization of a novel epoxy-based nanocomposite using tryptophan as an ecofriendly curing agent, Thermochem. Act. 574 (2013) 38–46.
[14] Y. Li, F. Xiao, C.P. Wong, Novel, environmentally friendly crosslinking system of an epoxy using an amino acid: tryptophan cured diglycidyl ether of bisphenol A epoxy, J. Polym. Sci., Part A: Polym. Chem. 45 (2007) 181–190.
[15] I. Isik, U. Yilmazer, G. Bayram, Impact modified epoxy/montmorillonite nanocomposites: synthesis and characterization, Polymer 44 (2003) 6371–6377.
[16] T.B. Tolle, D.P. Anderson, Morphology development in layered silicate thermoset nanocomposites, Key Eng. Mater. 62 (2002) 1033–1041.
[17] I.J. Chin, T.A. Thomas, H.C. Kim, T.P. Russell, J. Wang, On exfoliation of montmorillonite in epoxy, Polymer 42 (2001) 5947–5952.
[18] A.S. Zerda, A.J. Lesser, Intercalated clay nanocomposites: morphology, mechanics, and fracture behaviour, J. Polym. Sci., Polym. Phys. Ed. 39 (2001) 1137–1146.
[19] D. Duraibabu, M. Alagarb, S. Ananda Kumar, Studies on mechanical, thermal and dynamic mechanical properties of functionalized nanoalumina reinforced sulphone ether linked tetraglycidyl epoxy nanocomposites, RSC Adv. 4 (2014) 40132–40140.
[20] S.,L. Qiu, C.S. Wang, Y.,T. Wang, C.,G. Liu, X.,Y. Chen, H.,F. Xie, Y.,A. Huang, R.,S. Cheng, Effects of graphene oxides on the cure behaviors of a tetrafunctional epoxy resin, Express Polym. Lett. 9 (2011) 809–818.
[21] C. Alzina, N. Sbirrazzuoli, A. Mija, Epoxy-amine based nanocomposites reinforced by silica nanoparticles. Relationships between morphologic aspects, cure kinetics, and thermal properties, J. Phys. Chem. C 15 (2011) 22789–22795.
[22] A. Motahari, A. Omani, A.A. Rostami, Theoretical study on the mechanism of epoxy cured with tryptophan in the presence of 2,4,5-triphenylimidazole as a catalyst, Comput. Theor. Chem. 977 (2011) 168–180.
[23] B. Saha, A.K. Ghoshal, Model-free kinetics analysis of waste PE sample, Thermochim. Acta 451 (2006) 27–33.
[24] S. Vyazovkin, C.A. Wight, Model-free and model-fitting approaches to kinetic analysis of isothermal and nonisothermal data, Thermochim. Acta 340/341 (1999) 53–68.
[25] S. Vyazovkin, C.A. Wight, Kinetics of thermal decomposition of cubic ammonium perchlorate, Chem. Mater. 11 (1999) 3386–3393.
[26] K. Seefeldt, J. Miller, F. Alvarez-Núñez, N. Rodríguez-Hornedo, Crystallization pathways and kinetics of carbamazepine–nicotinamide cocrystals from the amorphous state by in situ thermomicroscopy, spectroscopy, and calorimetry studies, J. Pharm. Sci. 96 (2007) 1147–1158.
[27] D.R. Yei, H.K. Fu, W.Y. Chen, F.C.J. Chang, Synthesis of a novel benzoxazine monomer-intercalated montmorillonite and the curing kinetics of polybenzoxazine/clay hybrid nanocomposites, Polym. Sci. Polym. Phys. 44 (2006) 347–358.
[28] P. Budrugeac, E. Segal, Some methodological problems concerning nonisothermal kinetic analysis of heterogeneous solid–gas reactions, Int. J. Chem. Kinet. 33 (2001) 564.
[29] C.D. Doyle, Estimating isothermal life from thermogravimetric data, J. Appl. Polym. Sci. 6 (1962) 639–642.
[30] X. Sheng, M. Aknic, M.R.J. Kessler, Cure kinetics of thermosetting bisphenol E cyanate ester, Therm. Anal. Calorim. 93 (2008) 77–85.
[31] C.T. Vijayakumar, S.,S. Rishwana, R. Surender, S. Vinayagamoorthi, S. Alam, Structurally diverse benzoxazines: synthesis, polymerization, and thermal stability, Des. Monomers Polym. 17 (2014) 47–57.
[32] R. Surender, A. Mahendran, A. Thamaraichelvan, S. Alam, C.T. Vijayakumar, Curing Studies of bisphenol a based bismaleimide and cloisite 15a nanoclay blends using differential scanning calorimetry and model-free kinetics, J. Appl. Polym. Sci. (2013), https://doi.org/10.1002/APP.38219.
[33] N.,K. Sini, A. Motohisa, E. Takeshi, Synthesis and properties of spiro-centered benzoxazines, Macromolecules **48** (2015) 7466–7472.
[34] J. Dunkers, H. Ishida, Vibrational assignments of 3-alkyl-3, 4-dihydro-6-methyl-2H-1, 3-benzoxazines in the fingerprint region, *Spectrochim. Acta*, Part A 51 (6) (1995) 1061–1074.
[35] T.D. Ngo, M.T. Ton-That, S.V. Hoa, K.C. Cole, Effect of temperature, duration and speed of pre-mixing on the dispersion of clay/epoxy nanocomposites, Key Eng. Mater. 69 (2009) 1831–1840.
[36] R. Surender, A.R. Mahendran, A. Alam, C.T. Vijayakumar, Indane-based bismaleimide and cloisite 15a nanoclay blends: kinetics of thermal curing and degradation of particulate nanocomposites, Polym. Compos. (2013), https://doi.org/10.1002/pc.22538.
[37] A. Motahari, A. Omani, A. Rostami, Theoretical study on the mechanism ofepoxy cured with tryptophan in the presence of 2,4,5-triphenylimidazole as a

catalyst, Comput. Theor. Chem. 977 (2011) 168–180.
[38] S. Zainuddin, M.V. Hosur, Y. Zhou, A. Kumar, S. Jeelani, Durability studies of montmorillonite clay filled epoxy composites under different environmental conditions, Mater. Sci. Eng., A 507 (2009) 117–123.
[39] S. Zainuddin, M.V. Hosur, Y. Zhou, A.T. Narteh, A. Kumar, S. Jeelani, Experimental and numerical investigations on flexural and thermal properties of nanoclay–epoxy nanocomposites, Mater. Sci. Eng., A 527 (2010) 7920–7926.
[40] D. Piazzaa, A.F. Baldissera, S.R. Kunsta, E.S. Riederc, L.C. Scienzad, C.A. Ferreirad, J.A. Zattera, Influence of the addition of montmorillonite in an epoxy powder coating applied on carbon steel, Mater. Res. 18 (2015) 897–903.
[41] T.P. Mohan, M. Ramesh Kumar, R. Velmurugan, Thermal, mechanical and vibration characteristics of epoxy-clay nanocomposites, J. Mater. Sci. 41 (2006) 5915–5925.
[42] H.L. Ma, X. Zhang, K. Lau, S.Q. Shi, Effect of nanoclay concentration on the lap joint shear performance of nanoclay/epoxy adhesive at cryogenic condition, J. Compos. Mater. 52 (2018) 2477–2482.
[43] H. Czachor, Applicability of the Washburn theory for determining the wetting angle of soils, Hydrol. Process. 21 (2007) 2239–2247.
[44] A. Yasmin, L.,A. Jandro, M.,D. Isaac, Processing of clay/epoxy nanocomposites with A three-roll mill machine, MRS Proceedings 740 (2002), https://doi.org/10.1557/PROC-740-I3.7. I3.7.
[45] M.,W. Ho, C.,K. Lam, K.,T. Lau, Mechanical properties of epoxy-based composites using nanoclays, Compos. Struct. 75 (2006) 415–421.
[46] X. Xi, C. Yu, W. Lin, Investigation of nanographite/polyurethane electroconductive adhesives: preparation and characterization, J. Adhes. Sci. Technol. 23 (2009) 1939–1951.
[47] B. Guo, D. Jia, C. Cai, Effects. of organa-montmorillonite dispersion on thermal stability of epoxy resin nanocomposites, Eur. Polym. J. 40 (2004) 1743–1748.
[48] G. Sankar, N. Yan, Bio-based two component (2 K) polyurethane adhesive derived from liquefied infested lodgepole pine barks, J. Biobased Mater. Bioenergy 8 (2014) 1–8.
[49] H.,L. Tyan, C.,M. Leu, K.,H. Wei, Effect of reactivity of organics-modified montmorillonite on the thermal and mechanical properties of montmorillonite/polyimide nanocomposites, Chem. Mater. 13 (2001) 222–226.
[50] A. Motahari, A.,A. Rostami, A. Omrani, A. Ehsani, On the thermal degradation of a novel epoxy- based nanocomposite cured with tryptophan as an environment-friendly curing agent, J. Macromol. Sci., Phys. 54 (2015) 517–532.